

Magnetic Shield Design Modeling and Validation on SWOT Spacecraft Applied to Mars Flux Pinning Orbiting Sample Design

Edward Gonzales, Edward.C.Gonzales@jpl.nasa.gov
Boyan Kartolov, Boyan.Kartolov@jpl.nasa.gov
Laura Jones-Wilson, Laura.L.Jones@jpl.nasa.gov

Jet Propulsion Laboratory, California Institute of Technology

ABSTRACT

A modeling methodology was developed for use on the Surface Water and Ocean Topography (SWOT) mission for the computational modeling and design of a magnetic shield for a 63 A-m² source. Shield options were modeled and tested across various design parameters and validated with measurement. Measurement results fell within 10% of simulation in most cases of concern with sources of error well understood. These methods results informed a subsequent modeling activity for a future Mars Sample Return (MSR) mission concept with stringent magnetic cleanliness requirements to retain geologic integrity of the samples. One option for capturing the sample from orbit requires rare earth magnets in close proximity to the Martian samples. Magnetic modeling with a finite-element method solver estimated the magnetic environment and established the need for shielding. Further modeling then determined the shielding necessary to meet magnetic requirements, followed by the design of a mass-optimized solution.

KEYWORDS

magnetics, modeling, model validation, magnetic cleanliness, mars, flux pinning, sample return

INTRODUCTION

Magnetic cleanliness requirements are imposed on spacecraft for a variety of reasons spanning a need to protect component functionality from magnetic interference to a desire to limit the exposure of scientific samples/instruments to artificial magnetic fields. When these requirements constrain the design of a space system, it is necessary to have validated tools for evaluating magnetic field strength and, perhaps just as importantly, evaluating techniques for mitigating an existing field. This work describes the validation of one such magnetic modeling technique that was used to evaluate the shielding design for a set of strong permanent magnets on the Surface Water and Ocean Topography (SWOT) spacecraft. In this scenario, SWOT's Ka-band Radar Interferometer (KaRIn) instrument contains a set of two 63 A-m² permanent magnets in the two extended interaction klystrons (EIKs) that provide RF amplification. These magnets presented potential functional issues for nearby RF components, so the JPL engineers and EIK manufacturer proposed the use of magnetic shields to reduce the field at the susceptible components. The thickness (0.5 mm or 1.5 mm) and the material of the shield (cold rolled steel or mu-metal) were open trades that this modeling activity was intended to inform. This paper will first describe the

challenges in modeling magnetic shielding under intense magnetic fields and the model validation activity undertaken to garner confidence in the modeling methodology for the SWOT mission.

Once validated, this modeling technique was then applied to another example where strong fields generated by a set of permanent magnets must be mitigated to achieve the mission magnetic cleanliness requirements. In this application, a potential option for the capture and manipulation of an orbiting sample (OS) during a Mars Sample Return (MSR) mission concept involves using a flux-pinned interface (FPI) to manipulate the close-proximity dynamics between an OS and a sample return orbiter (SRO) (Davis et al. 1988). FPIs were first proposed by Cornell University as a technology where permanent magnets interact with field-cooled type-II superconductors such that the physics of magnetic flux pinning dominate their relative behavior (Shoer and Peck 2009, 57-65; Jones et al. 2010, 814-822; Shoer et al. 2010, 1066-1070; Jones et al. 2010, 8918; Jones and Peck 2011, 6703). In the proposed FPI-based approach to sample capture and manipulation, the sample cache shell (nominally a sphere for this study) is covered in an array of permanent magnets that interacts with a set of cryocooled superconductors mounted to a sample return orbiter. Prior to the rendezvous, the samples are collected by a surface mission, placed into the cache, and launched into a parking orbit. Then, the SRO rendezvous with the OS in Martian orbit in part by attracting the OS magnets into the potential well created by the trained superconductors. This non-contacting interface can be designed to generate a preferred equilibrium in both relative position and orientation, and maintain that equilibrium in up to six degrees of freedom without the use of any active control. As long as the superconductors remain below their critical temperature, the OS-to-spacecraft interface persists (Zhu 2016).

While flux pinning offers a number of advantages to close-proximity spacecraft operations, for a potential sample return application it also presents magnetic cleanliness challenges that requires mitigation in order to preserve the magnetic provenance (and thus maintain the scientific integrity) of the samples. Magnetic cleanliness programs typically mitigate strong magnetic sources by either taking advantage of the rapid decrease in field strength with distance from the source ($1/r^3$ for dipoles), the tendency for fields to be shunted by highly permeable materials (shielding), or for fields to cancel destructively (compensation). All of these options can result in an increase in mass, which is generally undesirable in an OS that must be launched into orbit from the Martian surface. This sensitivity to OS mass increases has made modeling the magnetic field – and the mass of mitigation strategies – particularly important when evaluating the resource costs of flux-pinning-based capture technology. Although many different potential OS designs may exist, the particular configuration and constraint set explored in this study limited the maximum diameter of the OS to 27 cm and called for a symmetric arrangement of twelve radially-facing permanent magnets around the outside shell of the OS. This configuration already yields the maximum benefit of field cancelation, and when coupled with the outer diameter limitation, shielding is the most promising mitigation strategy. This paper describes how the modeling lessons learned from SWOT were applied to the modeling of the magnetic field of the OS in order to establish the need for shielding, determine the feasibility of shielding to meet cleanliness requirements, and inform the trade between shielding mass and resulting field strength at the surface samples.

SWOT MODELING AND CALIBRATION

Magnetic modeling for the SWOT program was done in a commercially-available magnetic finite element model (FEM) solver. The FEM solver determines the shape and strength of magnetic fields by breaking the model geometry into a “mesh” of small fundamental 3D units—in this case, tetrahedra—within which it solves Maxwell’s Equations based on a set of input excitations. Within each mesh unit, material properties like permeability are taken into account. The initial mesh is solved with coarse mesh units during the first “solution pass” with an expectation that the mesh requires refinement in subsequent passes. Additional tetrahedrons are added with subsequent passes until convergence criteria are met on defined figures of merit (typically, percent change in field energy between solution passes).

Despite meeting convergence criteria, model fidelity is not guaranteed without accurate representation of the excitation. In order to accurately model the excitation, the two large permanent magnets in the SWOT EIKs were modeled as coils of wire on the order of the size of the physical magnets with current in the coils selected to generate a magnetic field that match the measured values of the real magnetic source (Figure 1). An engineering model EIK was measured with a single-axis axial gaussmeter probe in ~2 cm increments between approximately 8 and 25 cm along the z-axis shown in Figure 2. This approach tacitly assumes that the majority of field generated by the permanent magnets is in the axial direction, and that the measurements were made without any alignment error relative to the pole of the magnet. The measured field values are shown in Figure 3 as open black circles connected by a black dashed line. The magnitude of excitation in the FEM model was then iteratively adjusted to fit the curve shown by measurement. Figure 3 shows the simulated result as the solid black curve. Both curves agree to within 1-2 gauss at almost all data points in the measurement range, indicating that both the strength and general nature of the source are well modeled. The one-gauss discontinuity observed in the modeled curve at ~24 cm is believed to be an artifact of the FEM solver as a result of the imported geometry.

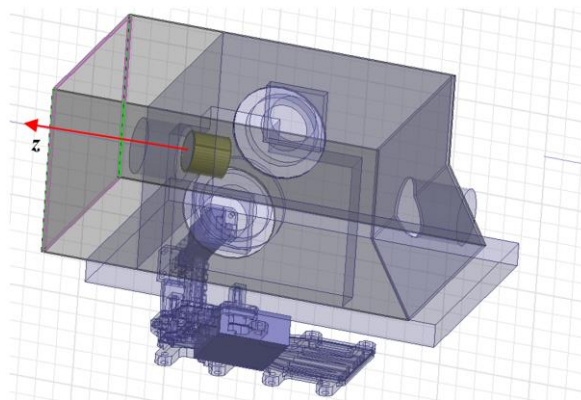


Figure 1. EIK model: magnet model in gold, conformal shield in gray

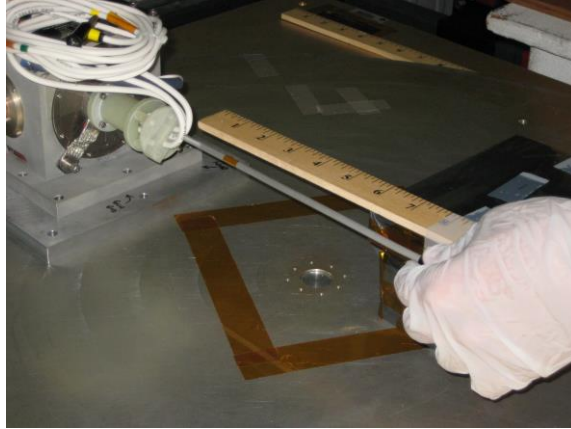


Figure 2. Measuring EIK without shield along magnet dipole, axial component

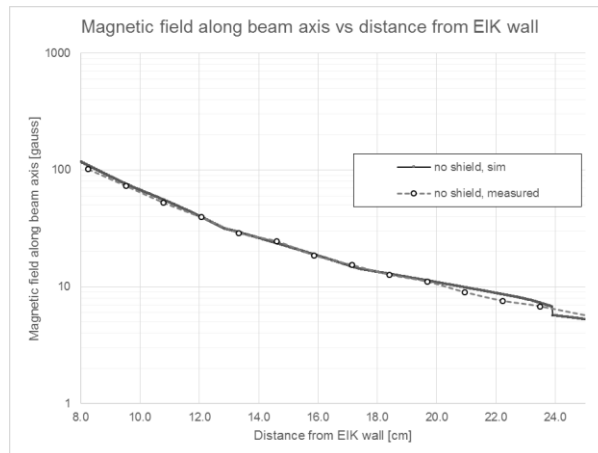


Figure 3. Magnetic field [gauss] vs. distance [cm], no-shield simulated and measured, axial component only

PROTOTYPE SHIELD MODELING AND TESTING FOR SWOT EIK

Once an accurate excitation was established, magnetic shields were designed and modeled per the open design trades: 1) 0.5 mm or 1.5 mm thick shielding, 2) mu-metal or 1010 cold-rolled steel. Two thicknesses were pursued in the hope that the thinner (and less massive) shielding option would be sufficient. An “open-topped box” design was assumed sufficient given the assumed direction of the dipole. Additionally, while the actual implementation will more-closely conform to the EIK shape, a simple box was used so that they could be built relatively easily to validate the modeling results.

Mu-metal and cold-rolled steel are common magnetic shielding materials with slightly different magnetic properties. Shielding materials generally have two parameters of concern: relative

permeability μ_r and saturation flux density B_{sat} . Relative permeability measures how well a material's microscopic domains respond to the presence of an external magnetic field while saturation flux density measures the external field above which a shield becomes ineffective. Shielding improves when either parameter increases. Mu-metal has a μ_r ranging between 7×10^4 and 1×10^5 but saturates at field strengths above about 0.7 T. On the other hand, 1010 cold-rolled steel has a significantly lower μ_r on the order of 7×10^2 but remains effective for field strengths in excess of 2 T. The primary goal of this modeling activity was to determine which of these competing parameters dominates for this geometry.

In order to model material permeability correctly, two changes to default simulation parameters are required: 1) reducing nonlinear residual and 2) extending shield material B-H curves. The nonlinear residual setting impacts the accuracy with which the modeler chooses a value from the material B-H curve. This value defaults to 10^{-3} in the software and was reduced to 10^{-7} for this model. Additionally, under high field strengths, the location on the B-H curve may lie well beyond what is specified in the standard material models and so must be extended to improve the B-H curve extrapolation accuracy in the FEM software. The existing material curves were exported as text files, additional data points were linearly extrapolated to extend the curves in the saturation regime, then the curves were imported back into the FEM software (Figure 4).

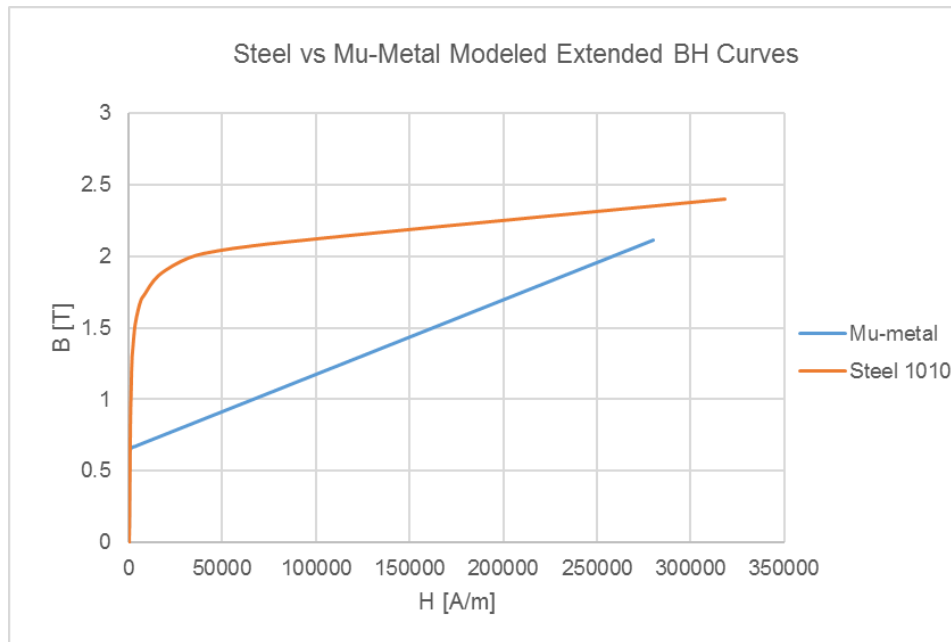


Figure 4. Modeled B-H curves for 1010 cold-rolled steel and mu-metal

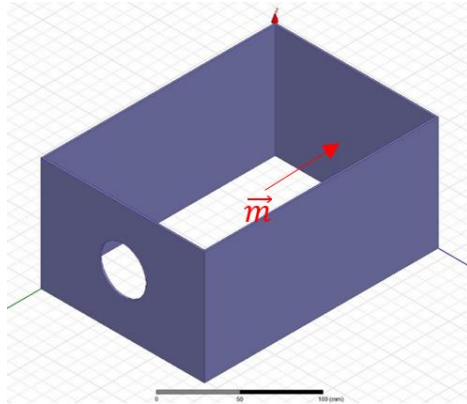


Figure 5. Open-topped shield design with magnet dipole shown in red

Once the shields were modeled, prototypes were built in order to validate the results. The exact nominal thicknesses for each material were not readily available, so the nearest available combinations were used: 1010 cold rolled steel in 0.43 mm and 1.58 mm, and mu metal in a single and double layer of 0.64 mm (double layer as a stand-in for the modeled 1.5 mm. Double layer was modeled later as an additional test case). Measurements were then taken along the magnetic dipole axis in the same locations as the no-shield condition.



Figure 6. Built open-topped shield, 1010 cold rolled steel, 0.43 mm

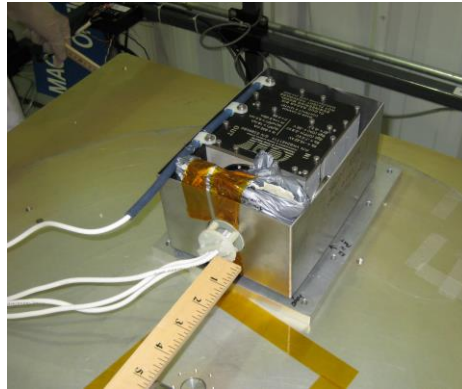


Figure 7. EIK with 1.58 mm steel shield

TEST RESULTS ON SWOT EIK

On-axis measurement results between 8 and 24 cm are shown in Figure 8. Nominal material thicknesses are referenced in the legend (e.g. 0.5 mm intended thickness instead of 0.43 mm actual). Solid lines indicate simulated values and dashed lines with discrete points are measured values. Error associated with shielding materials is shown in Figure 9.

Simulated results show a significant variation in the error in the close-field (closer than 14 mm from the EIK), and in this region the errors even switch sign, indicating that in some cases the simulated values are less conservative than the measured values. The fields in this region (especially within 10 mm) are more complex and so a single-axis probe would be expected to have significantly more negative error as a result. Spot checks performed with a three-axis probe showed that measurement converged to within 1.5 gauss of the simulated values at 16 cm and to within 4 gauss for points inside 11 cm (Gonzales and Mcwatters 2016, 23). However, the errors get significantly smaller beyond 14 mm from the EIK, where even the configuration with largest error (1.5 mm steel 1010) still shows a < 5 gauss difference between the measured and simulated results. In this range, most of the results show that the simulation overestimates the field at each point, but there are cases where the measured value was larger even in this region. Thus, for very tight cleanliness requirements a higher margin might be advisable to account for this potential lack of conservatism in the simulated values.

The results of this trade study also show that both mu-metal and steel reduce the apparent field of the system. In particular, for these strong magnetic fields, steel was better at reducing the field than mu-metal for similar thicknesses (even accounting for the fact that the actual steel plate was thinner than the nominal value and the mu metal was thicker than the nominal value). The 1.58 mm steel shield was the most effective at reducing the magnetic field of the options studied, so the SWOT project ultimately pursued the recommended shield configuration from this activity for maximum magnetic cleanliness: a 1.5 mm thick 1010 cold-rolled steel shield.

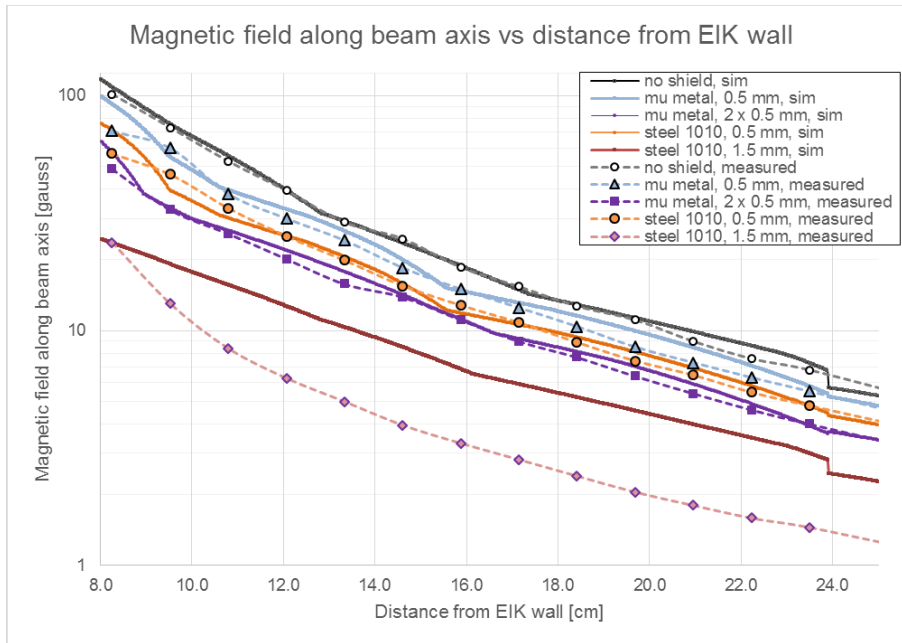


Figure 8. On-axis measurement results, axial component only

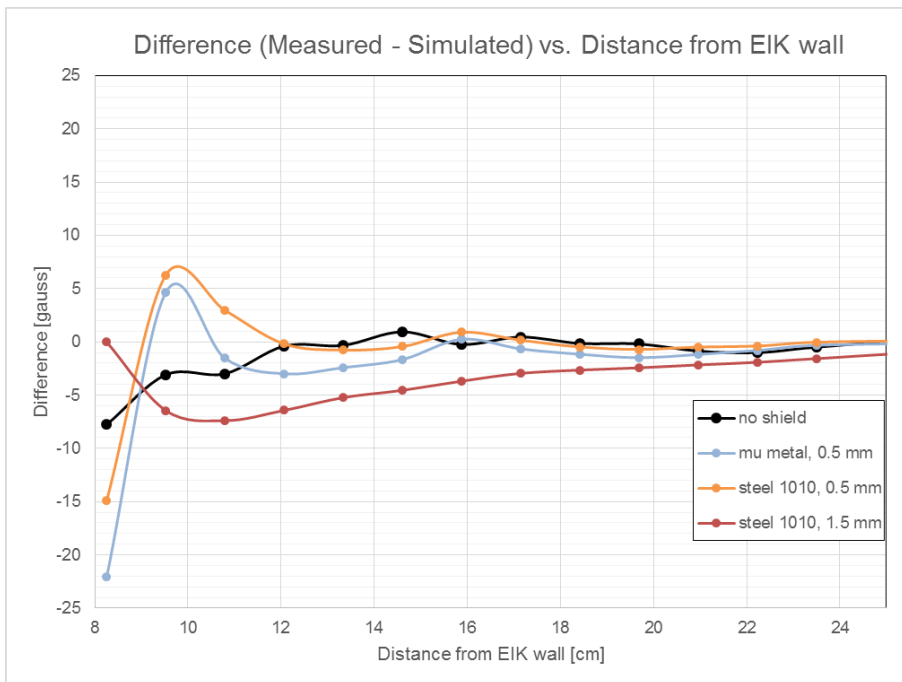


Figure 9: Difference [gauss] vs. distance from EIK wall [cm] for nominal test cases.

MODELING FOR POTENTIAL SAMPLE CAPTURE FPI

After establishing sufficient confidence in the high-field shield modeling techniques used to evaluate the SWOT EIK models, this same approach was used to evaluate the shielding options to preserve the magnetic provenance of the samples in a sample return cache that uses a flux-pinned interface for the sample capture and manipulation phase of a potential MSR mission. As shown in the concept art in Figure 10, the notional orbiting sample cache design is a sphere containing a set of sealed tubes with core samples from the Martian surface. For the FPI-based capture approach, the OS surface would place 12 evenly-spaced rare-earth magnets on the surface of a 27 cm sphere so that those magnets can interact with the other half of the interface on the SRO during the retrieval phase of the mission.

The magnetic field of a Martian core sample can serve as a window into the geologic past of Mars and the formation of the planet. Based on the expected magnetic coercivity of the samples, the science definition team established that 2 gauss (0.2 mT) would be allowed before the sample becomes adversely magnetized (Mustard et al 2013, 89). However, because the drilling hardware could expose the samples to 5 gauss (0.5 mT) during the collection process, the maximum magnetic exposure of the samples from the FPI hardware is limited to this value. The purpose of this study was then to determine if it is feasible to meet this requirement, and if so, how much mass in shielding would be required to attain it.

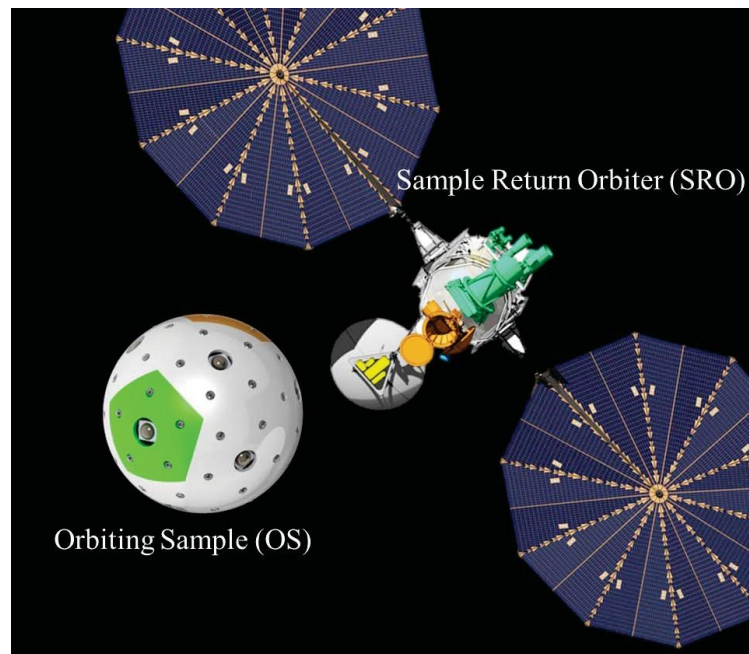


Figure 10. A conceptual sample-capture flux-pinned interface where the surface of the orbiting sample cache (OS) is populated with permanent magnets that interact with trained superconductors on the sample return orbiter (SRO) to generate a contactless, passively stable interface.

The OS geometry model was imported into the FEM software, which included models of the tubes containing Martian samples and defined the keep-out zone (KOZ) for fields in excess of the 0.5 mT requirement (Figure 11). The sources in the model are 12 NdFeB N42 spherical 0.75 inch

diameter magnets placed in a dodecahedron arrangement around the sphere with all dipole moments pointing to the center of the sphere, as shown in Figure 12. The modeled magnets featured a measured dipole moment = $3.3 \text{ A}\cdot\text{m}^2$ and a resultant surface B-field = $\sim 8000 \text{ gauss} = \sim 0.8 \text{ T}$. Whereas SWOT models used coils of wire to emulate the EIK permanent magnets given the analogous geometries, FPOS models utilized an appropriate permanent magnet material model that closely matched the nominal magnet strength (Figure 13).

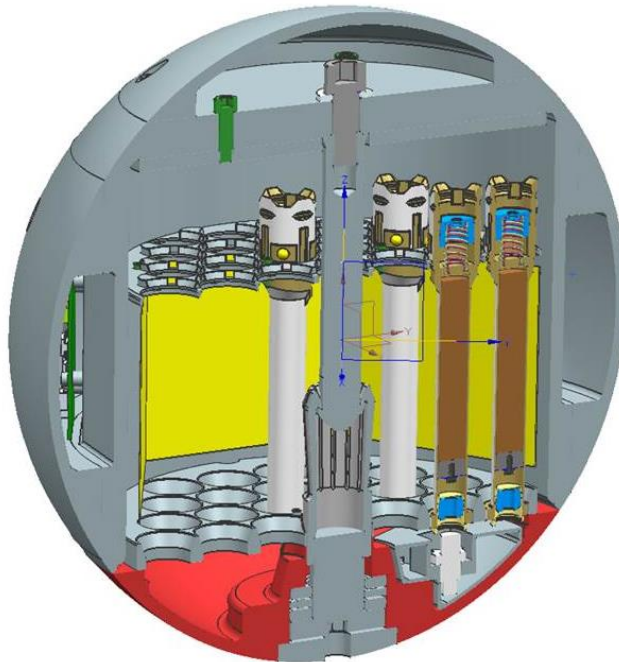


Figure 11. Cutaway of preliminary FPOS sample return sphere design with samples shown in brown and keep-out zone exterior (KOZ) in yellow. Magnets are not shown.

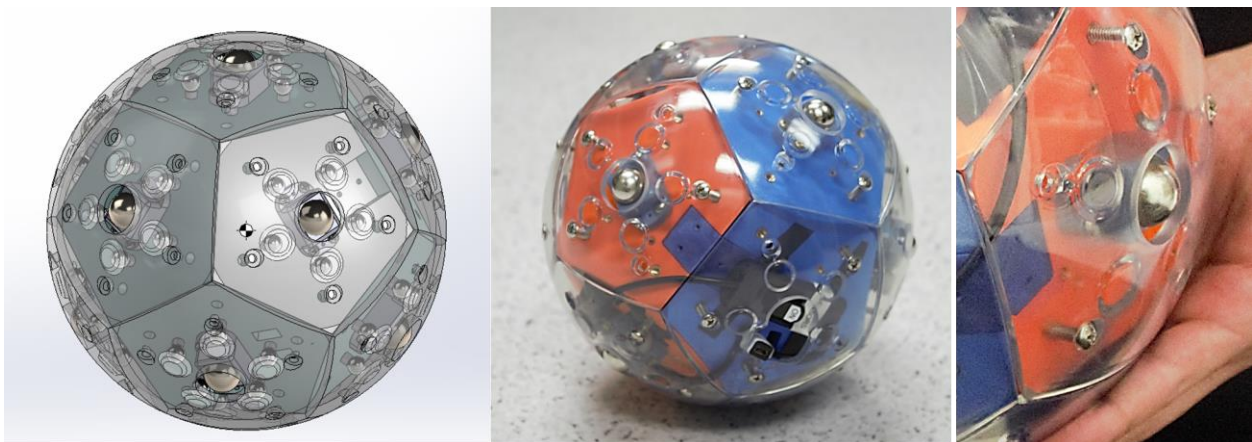


Figure 12: A hardware analog of the OS built to support ground testing of the FPI concept for sample capture applications, showing the locations of the spherical Neodymium magnets at each face of a dodecahedron.

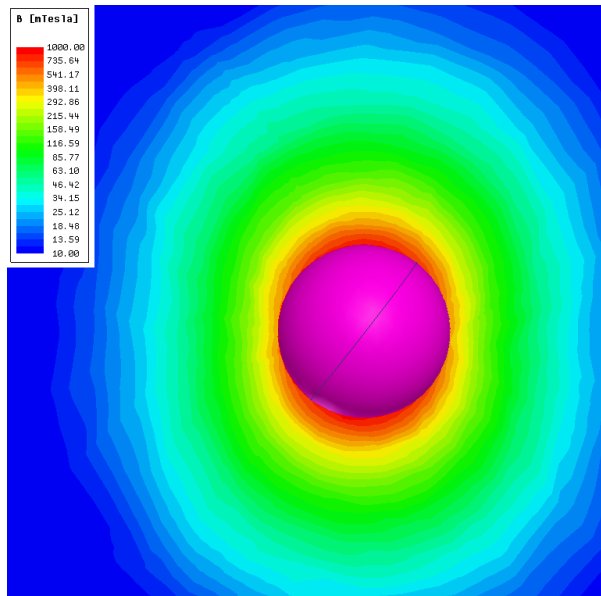


Figure 13. Modeled spherical rare-earth magnet calibrated to nominal strength

Initial activities focused on modeling the baseline configuration (no shielding) in the sample cache in order to understand the scope of the violations and guide any mitigation strategies. Figure 14 shows cut planes of the modeled baseline magnetic environment with the KOZ outlined in red toward the center of each cut plane. The color scale in all remaining plots is such that the 5 gauss requirement is met wherever the plot is dark blue. It can be seen that the baseline environment has several intrusions >15 gauss into the KOZ but are almost entirely on the KOZ periphery, hinting at the possibility of a feasible shielding approach.

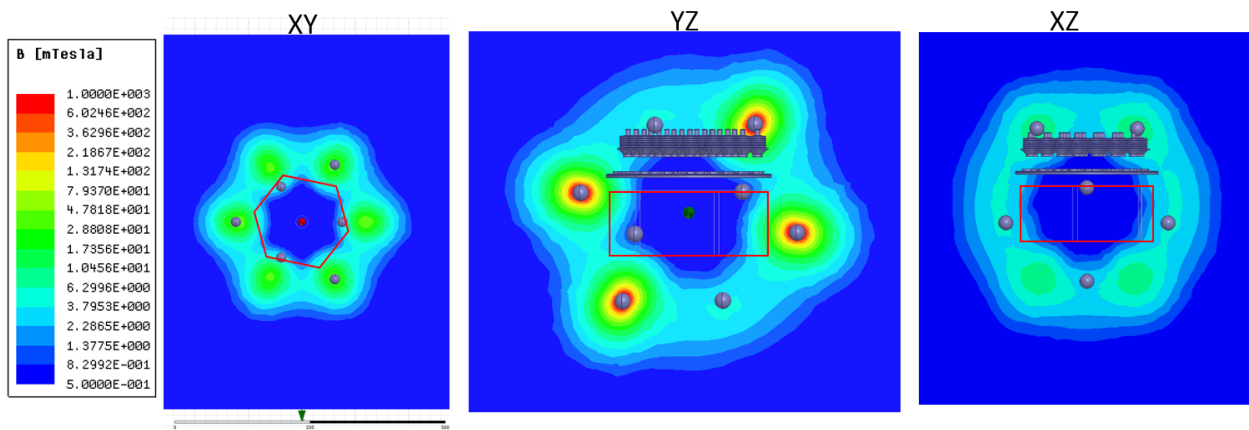


Figure 14. Baseline magnetic environment. KOZ outlined in red. Dark blue regions (lowest indicator on the scale) indicate where the 5 gauss requirement is met.

In evaluating the shielding options, cold-rolled steel and mu-metal were again proposed as potential materials. However, unlike SWOT, unique mechanical considerations immediately ruled out the use of mu-metal. The final stage of MSR would be entry, descent, and (potentially hard)

landing on Earth, which unsurprisingly imposes extreme mechanical shock on the FPOS. Mechanical shock disrupts the crystalline structure of nickel-iron alloys like mu-metal and thus adversely alters its magnetic properties (Wasilewski 1972). This, coupled with the success of steel shielding in high field environments as demonstrated in the SWOT study, steel was evaluated for use in this shielding application. This evaluation only considers the properties of steel at room temperatures for which B-H curves were available and assumed to provide a reasonable estimate at a median environment. Future studies could consider the impact of temperature of the sample magnetic cleanliness.

OS MAGNETIC SHIELD DESIGN

Because the Mars Sample Return concept scenario under consideration calls for launching the OS cache into Mars orbit from the surface and then returning to Earth via a re-entry vehicle, every gram is scrutinized. In order to limit the amount of additional material needed just for shielding, the design approach tried to capitalize on existing structures within the OS and simply replace aluminum with shielding-appropriate materials. As a first pass, a cylindrical aluminum canister surrounding the samples on all sides except the top was converted to 1010 steel in the FEM software. The resulting environment is shown in Figure 15 and is a marked improvement over the unshielded case. The incident field on the KOZ shows that requirement exceedances only occur on the unshielded side of the canister (Figure 16). A subsequent model added a steel lid to the canister and showed that the requirement was met at all locations on the KOZ. This approach of replacing existing geometry, however, has a significant mass penalty because it does not take advantage of the geometry that would be appropriate for the structural requirements given the new material properties. Thus, while it was determined that the requirement could be met within the existing volume constraints (addressing the feasibility question), the study then turned to assessing (and reducing) the mass impact from shielding.

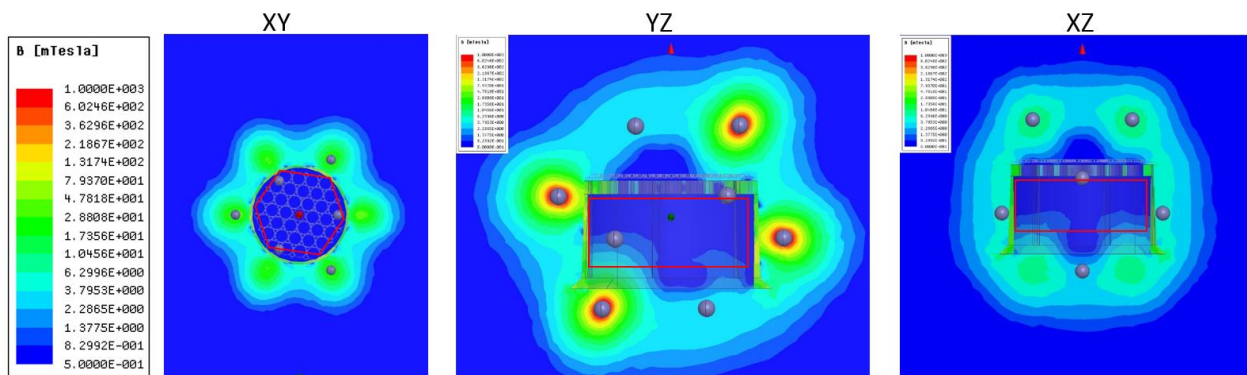


Figure 15. Magnetic environment when canister converted to 1010 steel.

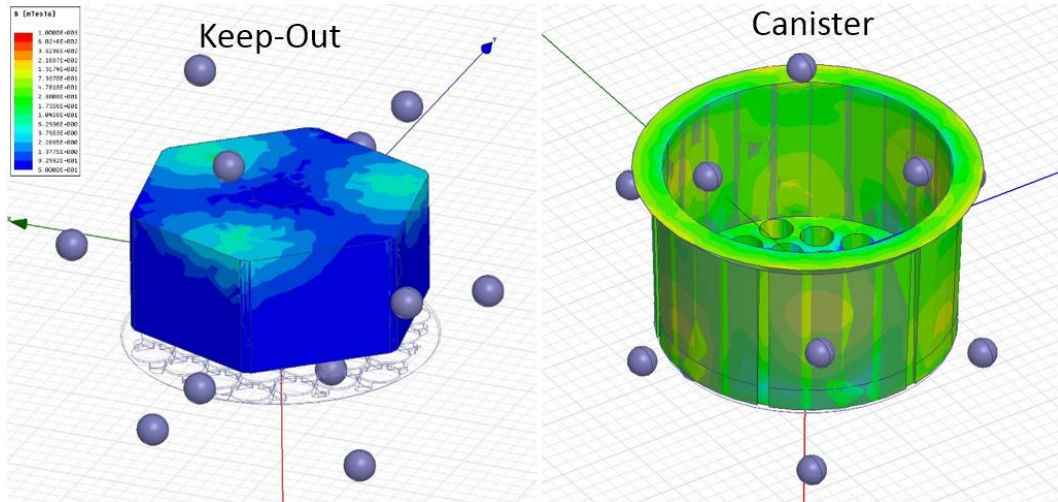


Figure 16. Left: incident field on KOZ on left. Right: Canister used as shield.

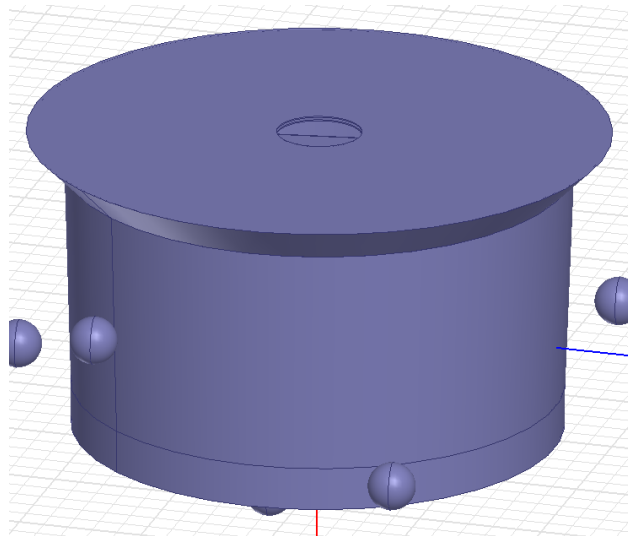


Figure 17. Cladded canister with lid.

After some iteration, it was discovered that cladding the outside of the canister in a single layer of 0.86 mm-thick steel at results in an approximately one kilogram mass penalty that meets the requirement in nearly all locations on the KOZ. However, additional reduction in the shield thickness resulted in clear requirement noncompliance; thus, for a single-layer steel shielding design, the lowest mass that still meets the requirement is likely on the order of one kilogram.

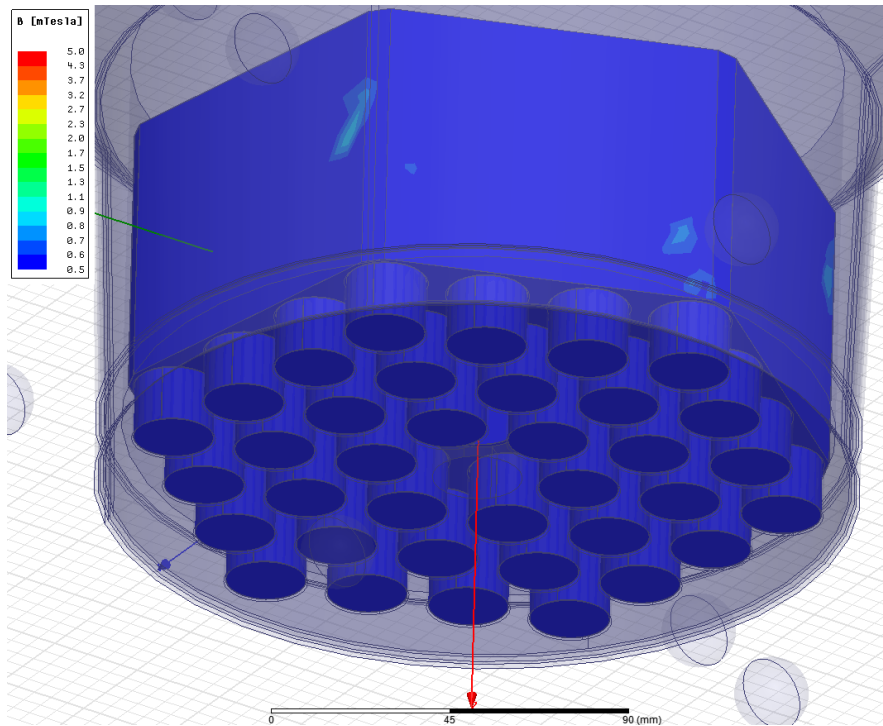


Figure 18. Field on KOZ exterior with a 1 kg single layer shield

Having reached the limit of a single layer shield design, a double-layer approach is the next level of shielding sophistication. Halving the thickness from the one kilogram in the single-layer design (0.43 mm) and cladding all interior and exterior surfaces of the canister effectively formed a 0.78 kg double-layer shield (including lid) (Figure 19). If 0.43 mm of aluminum is removed from the surface of the existing canister design and replaced by steel cladding, the net mass impact to the design is then 0.51 kg, meeting the mass target for the study.

Simulation of the double-layer shield performance showed that the 5 gauss requirement can be met on all surfaces of the KOZ (Figure 20). Exceedances can be seen on the bottom part of the KOZ, which is a result of holes in the shield needed to provide an insertion path for the sample tubes. The observed exceedances (~20 gauss) occur on portions of the sample tubes not containing core samples. While significant, the noncompliances are also highly localized: additional studies into the depth of these exceedances into the KOZ found that they did not impinge on the sample region and were deemed acceptable. While this design is preliminary and not yet validated by measurement, the results provided sufficient confidence in the flux-pinning approach to warrant further development. Additionally, the trade study here considered only mass and magnetic cleanliness, deferring considerations for manufacturability, structural integrity, and other implementation details for a later investigation.

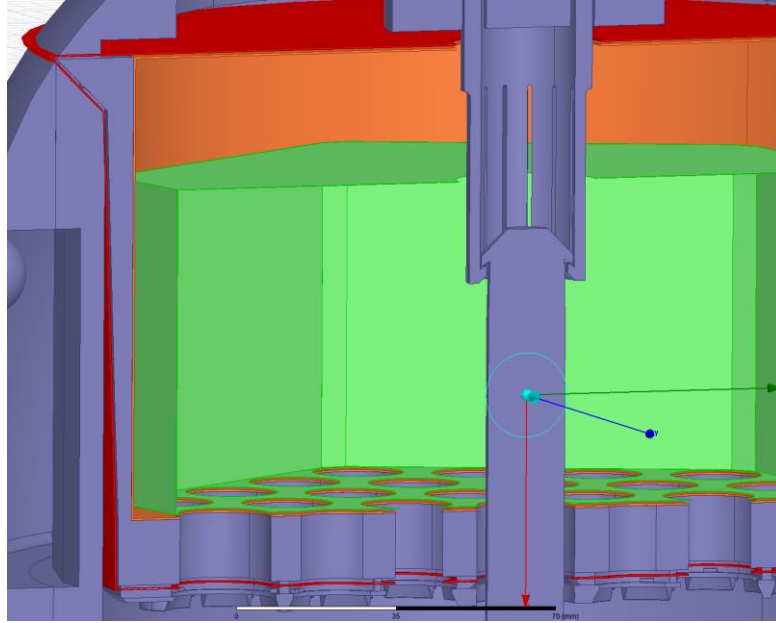


Figure 19. 0.78 kg 0.43 mm double-shield design (shown in red and orange)

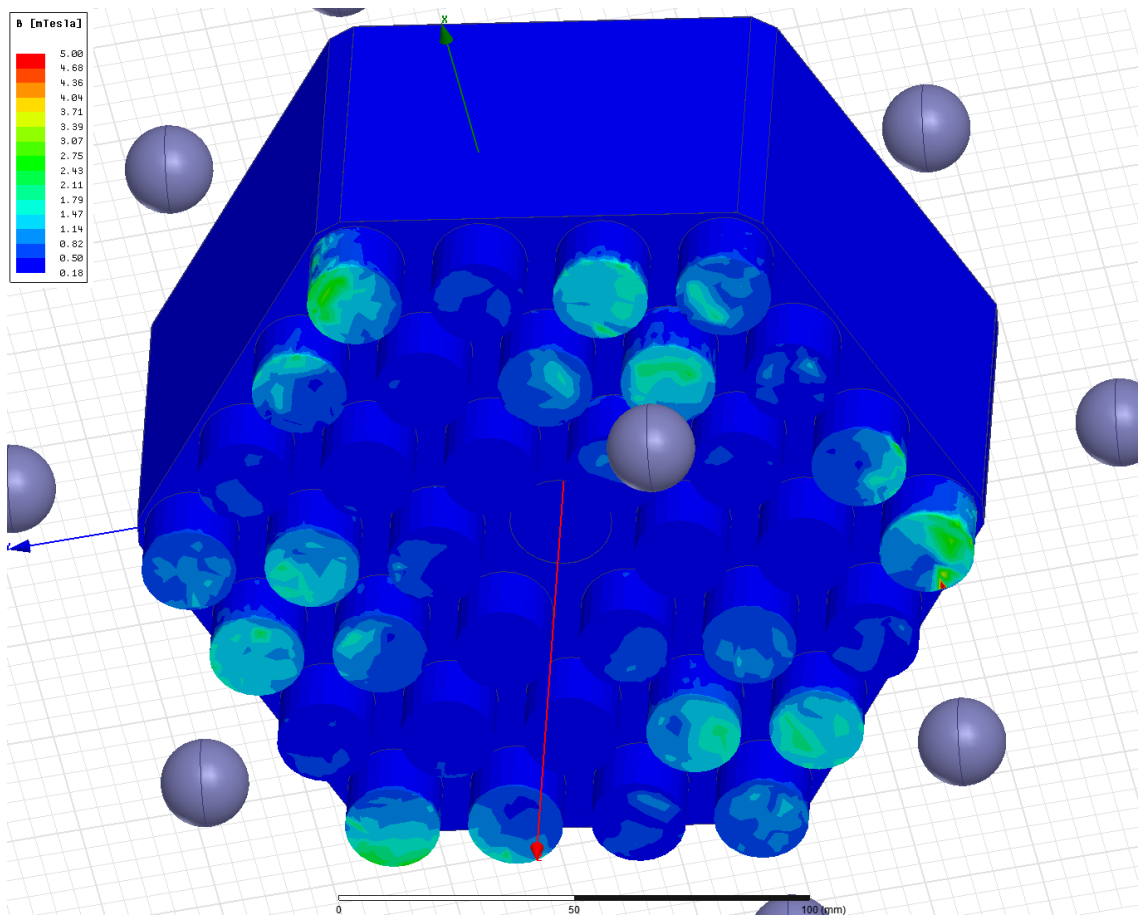


Figure 20. Magnetic environment on KOZ from 0.78 kg double shield. Exceedances on bottom of KOZ are on portions of sample tube not containing samples.

CONCLUSION

The magnetic modeling techniques developed in this paper for the SWOT mission and further applied to a potential Mars Sample Return flux-pinned interface capture technology demonstrated the ability to accurately design and model magnetic shields under high magnetic field environments. Careful configuration of the FEM simulation environment is necessary to ensure results that closely match measurement across a wide range of design variables: current-driven and permanent magnetic sources, simple and complex geometries, and differing shield materials and thicknesses. Once properly configured, magnetic FEM software can be a powerful tool for optimizing shield design and determining a spacecraft magnetic environment in ways that can powerfully shape the trade space for missions with magnetic sensitivities.

ACKNOWLEDGMENT

Nelson Huang provided the original EIK magnetic model and assistance in interpreting it.

Charles Rhoades from the JPL EMC Group assisted in taking magnetic measurements on the EIK.

David Rosing, Tomas Komarek, and Joseph Parrish for providing project support and input from the Mars office regarding requirements direction and trades of interest.

The work described in this paper was carried out at the Jet Propulsion Laboratory, California Institute of Technology, under a contract with the National Aeronautics and Space Administration.

COPYRIGHT

Copyright 2016 California Institute of Technology. U.S. Government sponsorship acknowledged.

REFERENCES

- Davis, L.C., E.M. Logothetis, and R.E. Soltis. 1988. "Stability of magnets levitated above superconductors." *Journal of Applied Physics*, vol. 64, no. 8, 4212.
- Gonzales, Edward C. and Dalia Mewatters. 2016. "Magnetic shield design modeling and validation for SWOT spacecraft Ka-band Extended Interaction Klystron." Proceedings of the *2016 IEEE International Symposium on Electromagnetic Compatibility (EMC 2016), Industry Papers: 19-24*.
- Jones, Laura L., and M. A. Peck. 2011. "Control strategies utilizing the physics of flux-pinned interfaces for spacecraft." *AIAA Guidance, Navigation, and Control Conference*, 2011, 6703.
- Jones, Laura L., W. R. Wilson, and M. A. Peck. 2010. "Design parameters and validation for a non-contacting flux-pinned docking interface". *AIAA SPACE 2010 Conference & Exhibition*, vol. 8918.
- Mustard, J.F., M. Adler, A. Allwood, D.S. Bass, D.W. Beaty, J.F. Bell III, W.B. Brinckerhoff, M. Carr, D.J. Des Marais, B. Drake, K.S. Edgett, J. Eigenbrode, L.T. Elkins-Tanton, J.A. Grant, S. M. Milkovich, D. Ming, C. Moore, S. Murchie, T.C. Onstott, S.W. Ruff, M.A. Sephton, A. Steele, A. Treiman. 2013. "Report of the Mars 2020 Science Definition Team." http://mepag.jpl.nasa.gov/reports/MEP/Mars_2020_SDT_Report_Final.pdf
- Norman, M.C., and M.A. Peck. 2010. "Simplified model of a flux-pinned spacecraft formation", *Journal of Guidance, Control, and Dynamics*, vol. 33, no. 3, 814–822.
- Shoer, J., and M. A. Peck. 2009 "Stiffness of Flux-pinned for Virtual Structures for Modular Spacecraft." *Journal of the British Interplanetary Society*, vol. 62, no. 2, 57-65.
- Shoer, J., W.R. Wilson, L.L. Jones, M. Knobel, and M.A. Peck. 2010. "Microgravity demonstrations of flux pinning for station-keeping and reconfiguration of cubesat-sized spacecraft." *Journal of Spacecraft and Rockets*, vol. 47, no. 6, 1066–1070.
- Wasilewski, Peter. 1974. "Magnetic Remanence Mechanisms In Iron And Iron-Nickel Alloys, Metallographic Recognition Criteria And Implications For Lunar Sample Research." *The Moon* 9: 335-354.
- Zhu, Frances, L. Jones-Wilson, and M. A. Peck. 2016. "Capturing and Docking Spacecraft with Flux-Pinned Interfaces." Paper presented at the 67th International Astronautical Congress (IAC), Guadalajara, Mexico, September 26-30, 2016.

BIOGRAPHIES

Edward Gonzales has been an Electromagnetic Compatibility Engineer at NASA's Jet Propulsion Laboratory since 2014. He is co-lead EMC Engineer for the Mars 2020 Rover and provides support for SWOT, Europa, and selected cubesat missions. He received his B.S.E.E. (magna cum laude) and M.S.E.E. degrees with an electrophysics emphasis from the University of Southern California. He is a member of IEEE and HKN.

Boyan Kartolov has been an Environmental Requirements Engineer (ERE) for the Mission Environmental Assurance Office at NASA's Jet Propulsion Laboratory since 2014. He is deputy ERE for the Mars 2020 Rover and the lead ERE for ECOSTRESS. He received his B.S.M.E. from the University of California, Irvine and his M.S.M.E degree with emphasis in thermodynamics from the University of California, Los Angeles. He is a member of IEEE, TBP, and PTS.

Laura Jones-Wilson earned her Ph.D. in Aerospace Engineering at Cornell University, where she specialized in the dynamics and controls of space systems. She wrote her thesis on the application of flux-pinned interfaces for spacecraft to close-proximity spacecraft dynamics. She then joined JPL in 2012 as a guidance and control systems engineer, where in addition to work on various flight projects she continues her research and development work on flux-pinned interfaces with her partners in the Cornell University and the JPL Mars Program Office.